Future developments - Adaptive Optics Applied to Glaucoma Imaging

Adrian Bradu[1], Toco Y. P. Chui[2,4], Christopher Costa[1], Alfred Dubra[3], Donald C. Hood[4], Konstantin Kapinchev[1], Adrian Podoleanu[1], Richard B. Rosen[2, 4], Jingyu Wang[1],
John S. Werner[6], Robert J. Zawadzki[6]
[1] Applied Optics Group, School of Physical Sciences, University of Kent, Canterbury, CT2 7NH,UK
[2] New York Eye and Ear Infirmary of Mount Sinai, 310 East 14 Street, Suite 319SB
New York, 10003
[3]Medical College of Wisconsin, The Eye Institute, 925 North 87th Street
Milwaukee, WI 53226-4812
[4]Dept. of Psychology, Columbia University, 1190 Amsterdam Avenue, 406 Schermerhorn Hall MC 5501, New York, NY 10027
[5] Icahn School of Medicine at Mount Sinai, New York, NY
[6] Department of Ophthalmology & Vision Science, University of California, Davis,
4860 Y St., Suite 2400, Sacramento, CA 95817

Introduction

Scanning laser ophthalmoscopy (SLO)[1] and optical coherence tomography (OCT)[2] have substantially advanced ophthalmic imaging by improving the transversal resolution and axial resolution beyond that which can be achieved by the fundus camera. SLO improved the transversal resolution by using a small aperture in front of the photodetector and OCT improved the axial resolution by employing principles of coherence gating. Combining the two technologies into a single instrument produces an OCT instrument with the transversal resolution of an SLO but the finer axial resolution afforded by OCT principles, typically 5-10 μm or less. Transversal resolution of both SLO and OCT instruments is limited by the aberrations of the eye to more than 15 μm with a pupil size of less than 3 mm. Transversal resolution in both instruments can, in principle, be improved to less than 3 μm resolution by enlarging the beam diameter. In practice, this often fails due to imperfections in the crystalline lens, cornea, intraocular fluid, and tear film that disturb the wavefront, and hence distort the round uniformity of the spot illuminating the retina. Applying adaptive optics (AO) principles, aberrations of the eye can be both measured and compensated.

Figure 1 illustrates a closed loop AO system. An AO loop consists of a Wavefront Sensor, which detects the aberrations of the light travelling through the eye, a Corrector, and a Feedback Loop, which signals the deformations to be applied to the Corrector. Correctors most commonly are deformable mirrors, with arrays of pistons that subdivide the reflective surface. Liquid crystals have also been used as Correctors, but they are limited in their range of correction and to certain polarization orientations, making them less suitable for imaging the retinal nerve fibre layer (RNFL).

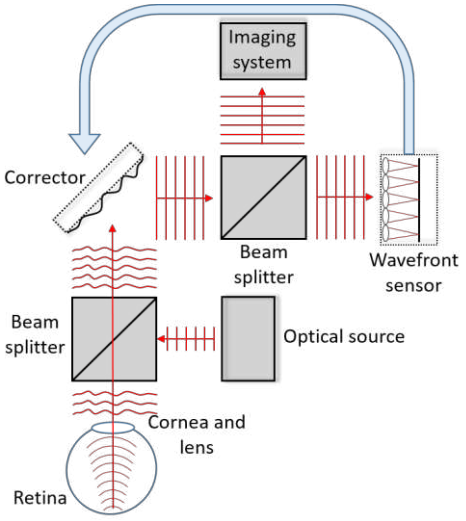

Figure 1. Schematic diagram of a closed loop adaptive optics system. The imaging system can be a fundus camera, an SLO, an OCT system, a fluorescence receiver or a combination of some or all of these.

Once the loop is operational, multiple beams can be adjusted with the same Corrector, serving functions, such as a fundus camera, an SLO, an OCT, a fluorescence channel or a multimodal instrument with a combination of imaging channels.

One of the major driving forces for developing AO for the eye was to image photoreceptors for diagnosis of patterns of photoreceptor loss in inherited and traumatic retinal disease and for monitoring therapeutic interventions. Recently, several groups have turned their attention to the inner retina, producing more than 35 glaucoma publications on studies of the optic nerve head (ONH) and the RNFL.

AO Imaging for Glaucoma

AO-SLO in diagnosing glaucoma

Current AO-SLO systems can visualize the RNFL bundles in patients with glaucomatous damage as well as in healthy controls (Figure 2)[3], enabling structural and functional studies of longitudinal changes due to glaucoma[4] at the interface between healthy and abnormal retina regions in the macula. Additionally, 3D characterization of the healthy human lamina cribrosa has attempted to quantify pore diameter, pore area, and pore aspect ratio as well as the connective tissue volume fraction[5].

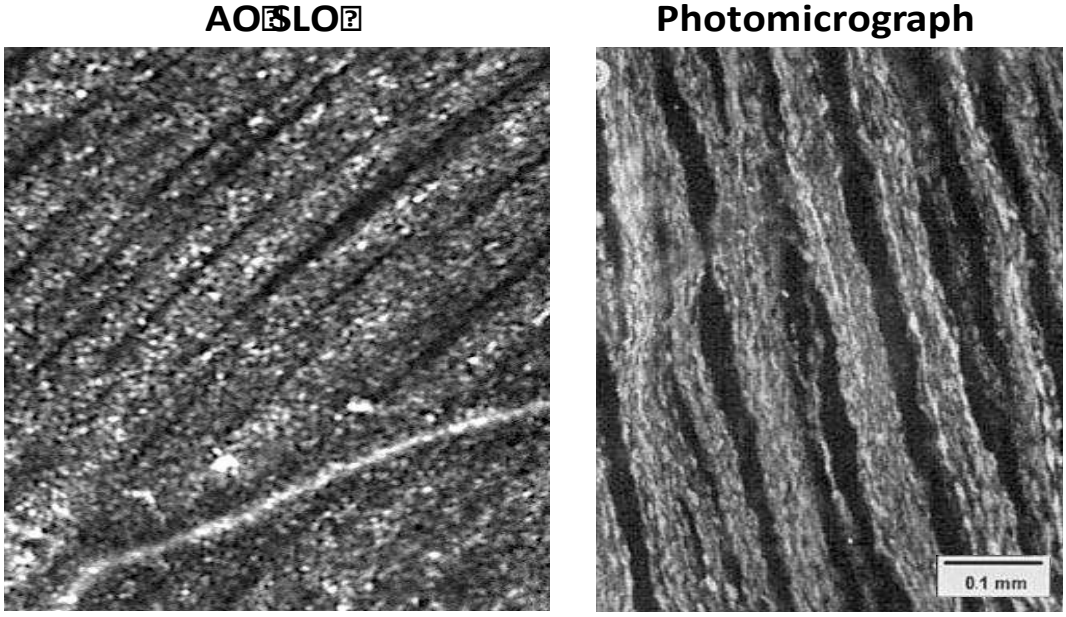

Figure 2. AO-SLO reflectance image of healthy individual retinal nerve fibers (left) compared to a transmission photomicrograph (right). Both images show bright spots within the bodies of the nerve fibers, described as axonal varicosities, which are believed to represent mitochondrial collections[6]. (AO SLO: unpublished image courtesy of Alfredo Dubra).

Hood et al.[3] compared AO-SLO images and OCT circular disc scans in patients with relatively similar deep, central arcuate defects. AO-SLO images revealed details of glaucomatous damage that were difficult, if not impossible, to detect with current OCT technology. Figure 3A shows a montage of AO-SLO images obtained near the optic disc of a patient with glaucomatous damage. For comparison, Figure 3B is the temporal half of a circumpapillary OCT scan of the same patient obtained for the region shown by the black semi-circle in Figure 3A. The purple arrows show corresponding blood vessel locations. It is clear that details in RNFL bundles seen in Figure 3A cannot be resolved in Figure 3B. This is in part due to the superior lateral resolution of the AO-SLO and in part due to the fact that there is information in local intensity differences, as well as thickness. These intensity variations will be completely missed with typical OCT circle scan analysis of RNFL thickness such as seen in Figure 3C. For example, the yellow arrow in Figure 3A indicates two RNF bundles sandwiched between regions devoid of RNF bundles and the yellow arrows in Figure 3C show the same location.

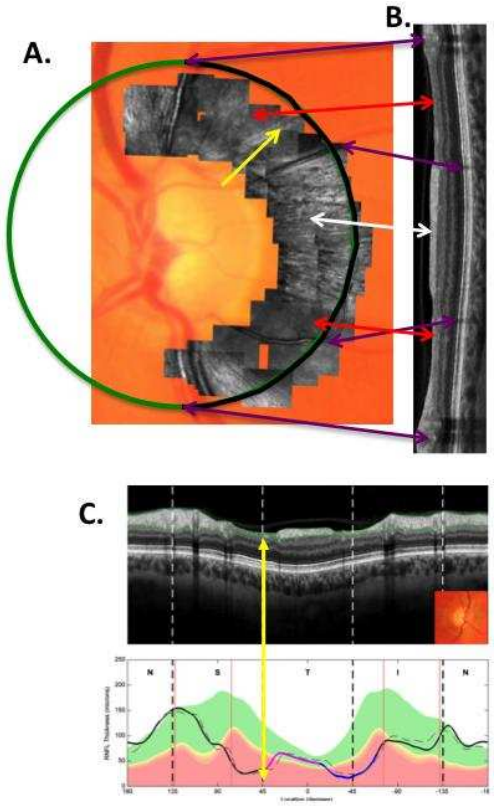

Figure 3.
A. A montage of AO-SLO images near the disc.
B. The OCT image from a circle scan around the disc. The black semi-circle in A is the location of the OCT image in B. The purple arrows show corresponding locations of blood vessels. The white and red arrows show corresponding locations of severely damaged (red) and relatively healthy (white) regions.
C. The OCT image of the complete circle scan of the disc (upper panel). The yellow arrowheads show the same location as the yellow arrow in panel A, which points to a region with two preserved RNF bundles. The lower panel shows the RNFL thickness (black curve) around the disc compared to normative values (shaded colored regions).

AO-SLO imaging is not ready for routine clinical use, requiring too much time and being limited to patients with good fixation, few lens changes, and low refractive error. However, it shows great promise for targeted trials looking for early evidence of progression of glaucomatous damage in limited numbers of patients. The details revealed by AO-SLO imaging should help us better understand the dynamic microanatomy of glaucomatous damage, as well as how best to detect such damage with OCT.

AO-OCT in quantifying glaucoma

OCT axial resolution depends on the spectral bandwidth of the light source, and is generally independent of lateral resolution. However, with broadband light sources ($\geq$ ~100 nm) and imaging beam diameters over 2 mm at the eye pupil, the effect of eye chromatic aberration becomes significant, resulting in blurring of the point spread function (PSF) and reduction of retinal image quality.

The usable depth range in AO-OCT is limited to the area where lateral resolution is high. When optical aberrations are maximally corrected, the depth of focus is <100 µm (~3-4 times less than the retinal thickness) so that multiple images at a single location with different positions of focus are needed to have optimum lateral resolution throughout the retina or optic disk. Figure 4 shows an AO-OCT B-scan having isotropic resolution $\leq$ 3.5 µm[7] with the AO focus on the inner retina. This permits visualization of individual axon bundles, even bundles within bundles, in the RNFL. This image is from a 55-year-old volunteer with a normal retina. Using a similar AO-OCT system, Kocaoglu et al.[8] later demonstrated bundle losses in a glaucoma patient (similar to those seen in Figure 3).

An AO-OCT system was able to detect and quantify structural changes at the temporal raphe even when local functional loss was mild, suggesting the raphe as a site of potential interest for glaucoma research and clinical assessment[9]. Relative reflectivity and nerve fibre bundle density were used to generate a quantitative bundle index.

Figure 5 shows AO-OCT images from a glaucoma patient. At the bottom, AO-OCT B-scans focus on the outer retina revealing the continuous external limiting membrane (ELM) as well as the cone photoreceptors at the inner-/outer-segment (IS/OS) junction and the cone outer segment tips (COST). This allows length measurements of the ISs (ELM to IS/OS)

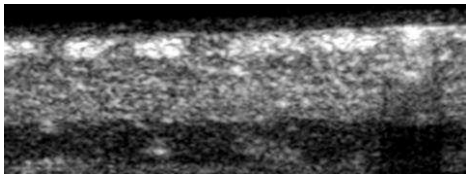

Figure 4: AO-OCT B-scan with focus on the inner retina of a 55-year-old normal observed over a 0.5 mm region of retina (9° superior, 4.5° nasal). This image is an average of 10 B-scans, each with 500 A-scans[7].

and OSs (IS/OS to COST). This approach is useful when combined with fundus images of the optic disk and visual field sensitivities as shown. In areas with the expected thinning of the RNFL, there is also a reduction in cone photoreceptor density and outer segment length[10]. Similar results have been found for other long-standing optic neuropathies.

In addition to quantifying changes in retinal structures, it is important in glaucoma to image the lamina cribosa. It consists of a multi-layered porous network of collagen fibres through which ganglion cell axons and major blood vessels pass. Mechanical strain in the lamina cribosa, expected from elevations in intraocular pressure, may cause loss of axoplasmic and blood flow associated with glaucoma leading to a loss of ganglion cells. Imaging the lamina cribosa is particularly challenging, since it requires an axial depth range of >2 mm.

While spectral domain (Fourier domain) OCT is highly sensitive, it has the disadvantage of sensitivity decay with depth and duplication of image, when the optical path difference equals zero inside the tissue examined. Methods have been devised to eliminate the mirror images (complex conjugate artefact) and extend the axial range of the OCT channel. Such a method has been applied in imaging the lamina[11], thereby allowing structures of interest to be placed in the area of maximum sensitivity and at the same time doubling the axial imaging range.

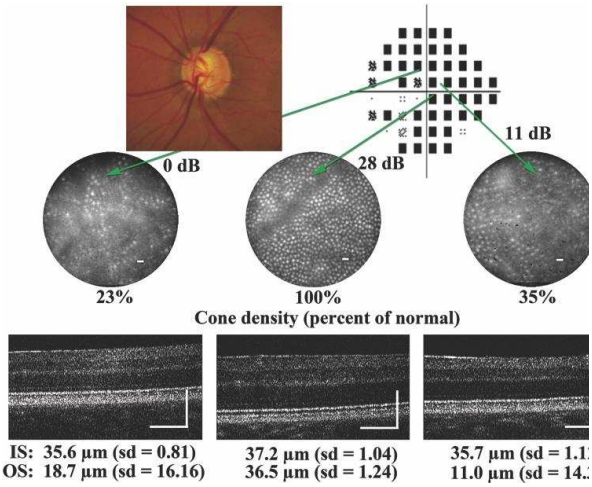

Figure 5: The fundus photo on the upper left shows the ONH of a 25-year-old patient with pigment dispersion glaucoma. The upper right shows his visual field in terms of total deviation plot. Visual field sensitivities show retinal areas for high-resolution imaging. The circular areas show the cone mosaic obtained in an AO-flood illumination image, with percentages indicating the proportion of cones expected in a normal retina. AO-OCT B-scans from the corresponding retinal locations are shown in the bottom row. Mean length of inner - (IS) and outer-segments (OS) of the cones are indicated for each retinal location[10].

Several methods have been used to remove the complex conjugate artefact. The images in Figure 6 were obtained with a reference arm-based phase-shifting method which acquires B-scans by means of consecutive A-scans that differ by a constant phase shift, allowing the reconstruction of the imaged structure with respect to the zero delay position. The figure shows C-scans of the lamina cribosa over a large depth range of a normal 60-year-old made possible by suppression of the complex conjugate artefact. The areas of eight lamina cribosa pores are identified at different depths from the interior to the exterior lamina. These in vivo results agree well with histological measurements from donor eyes. Volumetric analysis of the laminar structure may make it possible to investigate laminar beam networks as they are compressed or collapsed in advanced glaucoma. These tools may permit the evaluation of new therapeutic options and neuroprotective strategies in the treatment of glaucoma[12].

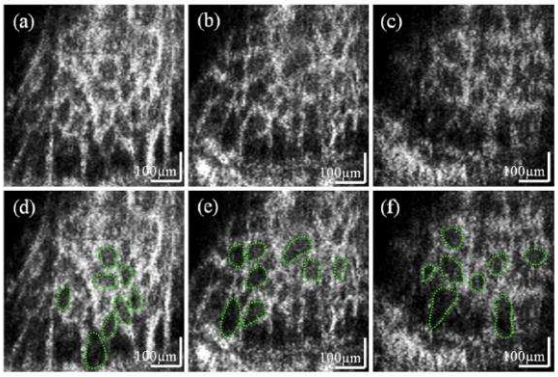

Figure 6: Lamina cribosa at different depths obtained with AO-OCT and suppression of the complex conjugate artefact. The locations are (a) 56 µm, (b) 108 µm, and (c) 145 µm from the anterior lamina surface. The eight pores in the bottom images allow segmentation and quantification through the lamina cribosa[11].

Limitations and caveats

Expanded implementation of AO faces a number of challenges. First, it is difficult to obtain acceptable images on patients with cataracts, dry eyes, small pupils, high refractive error, or with epiretinal membranes overlying the region of interest. Second, imaging time typically involves tens of minutes. Third, data analysis and assembly is time consuming. Since AO images are small in lateral dimension, multiple images from adjacent locations must be montaged with specialised registration software.

A major limitation that prevents wider commercialization of the AO technology is the large layout required, that demands a specialised optics lab.

Future progress in the imaging technology

Simultaneous display of en face images from different depths AO improves transversal resolution, enhancing the definition in en face views, while OCT mainly enhances cross sections. The conventional SDOCT, being based on A-scans, requires collection of the whole volume of data before cutting en face slices by software. A method that delivers the en face view directly has been recently developed, termed Master/Slave OCT[13]. This provides simultaneous multiple en face images from different depths, as shown in Fig. 7.

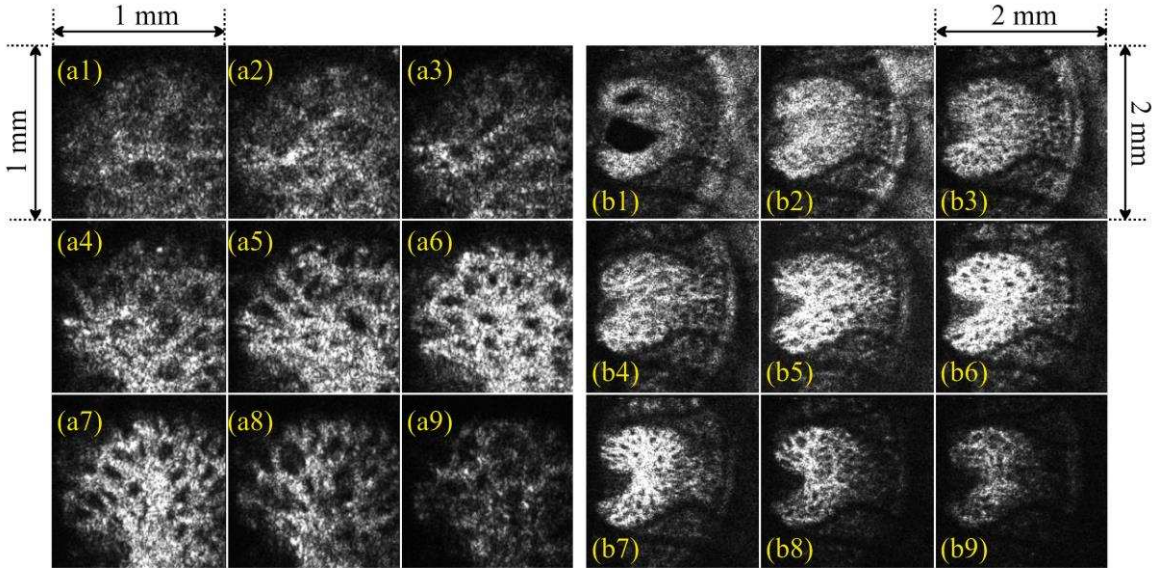

Figure 7. Nine en face images from the human lamina produced simultaneously, in vivo and in real time by using Master/Slave OCT technology[13] with different lateral size. In the left panel, the lateral size of the images is 1x1 mm while in the right panel 2x2 mm. In both panels, consecutive images are axially separated by 57.6 µm. All distances are measured in air. Only 9 images are shown; the technology allows more than 40 images to be produced simultaneously.

Sensorless plus corrector Eliminating the Wavefront Sensor (WFS) allows assembling the interface optics by using lenses making the system more compact and lower cost. Iterative algorithms are used to search correction space by applying different shapes to wavefront correctors to maximise intensity or sharpness, limited mainly by processing time. This has been addressed recently by using parallel processing in graphic cards to speed up the optimisation of signal sent to the corrector, allowing in vivo retinal imaging in experimental animals and more recently in the human eye[14].

Sensorless and correctorless A more adventurous AO solution involves eliminating the corrector and using the features in the images acquired to sense aberration. Such a configuration is based on subaperture AO, where the phase distortion is inferred from en face OCT images, followed by iterative computationally-added correction of aberrations[15].

Acknowledgments
National Eye Institute (R01 EY 024239). European Research Council (ERC) (http://erc.europa.eu) COGATIMABIO 249889, NIHR Biomedical Research Centre at Moorfields Eye Hospital NHS Foundation Trust and the UCL Institute of Ophthalmology, School of Computing at the University of Kent, EPSRC DTA funding, Wolfson research merit award. Marrus Family Foundation, Wise Family Foundation, Lowenstein Foundation, New York Eye and Ear Chairman's Research Fund, NEI U01 EY025477-01, Millbank Foundation, Research to Prevent Blindness.

References

[1] R. H. Webb, G. W. Hughes, and O. Pomerantzeff, "Flying spot TV ophthalmoscope," Appl. Opt. **19**, 2991-2997 (1980).
[2] D. Huang, E.A. Swanson, C.P.Lin, J.S. Schuman, W.G. Stinson, W. Chang, M.R. Hee, T. Flotte, K. Gregory, C.A. Puliafito, et al., "Optical coherence tomography," Science 254, 1178-1181 (1991).
[3] D. C. Hood**,** M. F. Chen, D. Lee, B. Epstein, P. Alhadeff, R. B. Rosen, R. Ritch, A. Dubra, T. Y. O. Chui, "Confocal adaptive optics imaging of peripapillary nerve fiber bundles: Implications for glaucomatous damage', Trans Vis Sci Tech. 4(2):12 eCollection (2014).
[4] T. Kostanyan, G. Wollstein, J. S. Schuman, "New developments in optical coherence tomography", Current opinion in ophthalmology. 26(2), 110-115 (2015).
[5] Z. Nadler, B. Wang, J. S. Schuman, R. D. Ferguson, A. Patel, D. X. Hammer, R. A. Bilonick, H. Ishikawa, L. Kagemann, I. A. Sigal, G. Wollstein, "In vivo three-dimensional characterization of the healthy human lamina cribrosa with adaptive optics spectral-domain optical coherence tomography", IOVS 55(10), 6459-6466, (2014).
[6] L. Wang, J. Dong, G. Cull, B**.** Fortune, G.A. Cioffi, "Varicosities of Intraretinal Ganglion Cell Axons in Human and Nonhuman Primates", Investigative Ophthalmology & Visual Science, January 2003, 44(1).
[7] R. J. Zawadzki, B. Cense, Y. Zhang, S. S. Choi, D. T. Miller, J. S. Werner, "Ultrahigh-resolution optical coherence tomography with monochromatic and chromatic aberration correction", Optics Express, 16, 8126-8143 (2008).
[8] O. P. Kocaoglu, B. Cense, R. S. Jonnal, Q. Wang, S. Y. Lee, W. H. Gao, D. T. Miller, "Imaging retinal nerve fiber bundles using optical coherence tomography with adaptive optics", Vision Research, 16, 1835-1844 (2011).
[9] G. Huang, T. Luo, T. J. Gast, S. A. Burns, V. E. Malinovsky, W. H. Swanson, H. William, "Imaging glaucomatous damage across the temporal Raphe", IOVS, 56(6), 3496-3504, (2015).
[10]J. S. Werner, J. L. Keltner, R.J. Zawadzki, S. S. Choi, "Outer retinal abnormalities associated with inner retinal pathology in nonglaucomatous and glaucomatous optic neuropathies", Eye, 25, 279-289, (2011).
[11] D. Y. Kim, J.S. Werner, R. J. Zawadzki, "Complex conjugate artifact-free adaptive optics optical coherence tomography of in vivo human optic nerve head", J. Biomed Optics, 17(12), 126005 (2012).
[12] E. R. Tamm, L. Schmetterer, F. Grehn, "Status and perspectives of neuroprotective therapies in glaucoma: The European Glaucoma Society White Paper", Cell and Tissue Research, 353, 347-354, (2013).
[13] A. Gh. Podoleanu and A. Bradu, "Master–slave interferometry for parallel spectral domain interferometry sensing and versatile 3D optical coherence tomography," Opt. Express **21**, 19324-19338 (2013).
[14]K. S. K. Wong, Y. Jian, M. Cua, S. Bonora, R. J. Zawadzki, M. V. Sarunic, "In vivo imaging of human photoreceptor mosaic with wavefront sensorless adaptive optics optical coherence tomography", Biomed Opt Express. 6(2): 580–590 (2015).
[15] A. Kumar, T. Kamali, R. Platzer, A. Unterhuber, W. Drexler, R. A. Leitgeb, "Anisotropic aberration correction using region of interest based digital adaptive optics in Fourier domain OCT," Biomed. Opt. Express 6, 1124-1134 (2015).